Eur. Phys. J. E (2012) **35**: 48
DOI 10.1140/epje/i2012-12048-3

THE EUROPEAN PHYSICAL JOURNAL E

Regular Article

Numerical deflation of beach balls with various Poisson's ratios: From sphere to bowl's shape

C. Quilliet[a]

Université Grenoble/CNRS, LIPhy UMR5588, Grenoble, France

Received 19 October 2011 and Received in final form 30 March 2012
Published online: 19 June 2012 –

Abstract. We present a numerical study of the shape taken by a spherical elastic surface when the volume it encloses is decreased. For the range of 2D parameters where such a surface may model a thin shell of an isotropic elastic material, the mode of deformation that develops a single depression is investigated in detail. It occurs via buckling from sphere toward an axisymmetric dimple, followed by a second buckling where the depression loses its axisymmetry through folding along portions of meridians. For the thinnest shells, a direct transition from the spherical conformation to the folded one can be observed. We could exhibit unifying master curves for the relative volume variation at which first and second buckling occur, and clarify the role of Poisson's ratio. In the folded conformation, the number of folds and inner pressure are investigated, allowing us to infer shell features from mere observation and/or knowledge of external constraints.

1 Introduction

Let us consider a thin shell of an elastic isotropic material, such as a beach ball, and deflate it. What would be its shape?

This question is not restricted to garrulous familial shores: fundamental and applied physics nowadays presents legions of easily deformable soft objects, and knowing what governs their shapes gives the powerful possibility of inferring mechanical properties from simple observations, without contact. Among these deformable objects, an increasing number derives from spherical symmetry, that is omnipresent at scales where surface effects overcome volume forces such as gravity. The numerical study presented in this paper discusses the shapes taken by spherical thin shells of isotropic materials when their inner volume is decreased by a significant amount. Such a systematic and quantitative study will help deciphering conformations observed in, *e.g.*, soft matter (lock-and-key colloids [1], multiwall capsules [2], particles design through evaporation [3, 4]), galenics (encapsulation [5]), microfluidics (microtanks [6]) or medicine (ultrasound contrast agents [7]), under the action of an external pressure or other possibly isotropic fields such as concentration in evaporation/dissolution phenomena, which also shapes objects in Nature [8].

When an elastic spherical shell has its inner volume lowered, it first deforms through in-plane compression that respects the spherical symmetry. Then it undergoes a symmetry breaking in order to relax a high stretch energy into much lower bending energy, by reversion of a spherical cap (creation of an axisymmetric depression, or "dimple"). The onset of this sudden transition, or buckling, under external pressure was studied long ago by Pogorelov and Landau [9,10]. They showed that the dimple should nucleate over a critical outside/inside pressure difference scaling like $Y_{3D}(\frac{d}{R})^2$ (in what follows, we will refer to this latter quantity by $\Delta P_{\mathrm{Landau}}$), where d is the shell thickness, R its radius and Y_{3D} the Young modulus of the material that makes it up. Its edge (or "rim") has a transversal extension $\sqrt{dR}$. One of the keys of their calculation being the assumption that buckling occurs for dimples such that maximum deflection is of order d, spherical geometry imposes then that $\sqrt{dR}$ is also the radius of the dimples that form. Besides, classical buckling analysis provided dependence of the buckling pressure on Poisson's ratio [9–11].

Results focusing on deformations through further deflation are, mainly, more recent. A few months ago, stability analysis allowed a detailed study of buckling toward axisymmetric conformations [12]. Experimental [1, 3, 13–17] and numerical [3, 17, 18] deflation studies showed shapes holding several dimples, also called "multiple indentation". These conformations compete with experimental observations of shapes holding a single depression [14, 16], possibly losing axisymmetry [19] or exhibiting folding perpendicularly to the rim [15, 20]. Similar shapes are observed in shells under a point load [21, 22] or pressed against a wall [22, 23]. Secondary buckling by folding

[a] e-mail: Catherine.Quilliet@ujf-grenoble.fr

of the single depression, also called "polygonal indentation", under isotropic constraint was numerically retrieved with surface models [18, 20]. Thin shells with a single depression, either axisymmetric or polygonal, appear to present a conformation of lower energy than the metastable multiple indentation [17, 18, 20]. In the case of an axisymmetric dimple, this can be easily understood since elastic energy mainly concentrates in dimple edges as bending energy, with an energy per edge length that weakly varies with dimple size. Hence coalescence of dimples lowers the total elastic energy[1]. Nevertheless, more than one dimple may nucleate if the deflation is rapid enough, leading to metastable [3, 17, 18] multi-indented shapes. The term "rapid" is to be taken on a wide acception here. Experimentally, it may correspond to situations where dissipation (due to material viscosity or to fluid flows accompanying the deformation) prevents dimple growth, which favors secondary nucleation once $\Delta P_{\mathrm{Landau}}$ is reached, and where subsequent kinetics prevents thermally activated coalescence between adjacent dimples. Numerically, minimization may reproduce such metastable situations [3, 17, 18], since: i) large volume increments favor the creation of extra dimples, by making it difficult to find the cooperative displacement of vertices that corresponds to rim rolling in dimple growth, ii) depending on the way curvatures are calculated, energy barriers that prevent from dimple coalescence may be overcome or not. For "slow" deflations, a single dimple can appear and grow, or freshly nucleated dimples may coalesce into a single one. Such "slow" deflation provides an axisymmetric bowl-like shape, that may undergo under further deflation a transition toward a non-axisymmetric depression, *i.e.* polygonal indentation [18, 20].

We present here a systematic numerical study of such "slow" deflations leading to shapes with a single depression. In this purpose, we used a surface model taking into account recent developments, presented in sect. 2. We clearly expose the correspondence between 2D parameters of the model surface, and 3D properties of the real object of non-zero thickness, expliciting the role of the different significative parameters. Particular emphasis is put on a parameter often underconsidered: Poisson's ratio.

The whole study allows to determine parameters of importance for the transitions sphere → axisymetric bowl (sect. 3) and axisymmetric bowl → polygonal indentation (sect. 4), both for the detailed shape in polygonal indentation, and for inner pressure. Furthermore, we took particular care in providing empirical dependence laws for practical use.

[1] Calculations of ref. [24] led to the inverse conclusion. With current hindsight, it appears that the elastic energy of large dimples (size approaching the shell's one) was overestimated in this paper. In the pure curvature model used in it, following ref. [30] the rim's curvature was estimated as $\sqrt{Rd}/\tan\alpha$, where α is the half-angle of the cone in which the dimples inscribes; this term caused a quick increase of the elastic energy with α. More recent calculations showed that lateral extension of the rim is better described by $\sqrt{Rd}/\alpha$ before autocontact [12]; this prevents multiple indentation from being of lower energy than single indentation in the pure curvature model.

2 Surface model

Surface model, where out-of-plane and in-plane deformations are formally uncoupled, has long been considered as valid to describe the deformation of thin sheets (plates or shells) [10, 25]. For thin sheets without spontaneous curvature (*i.e.* an elementary surface portion of the sheet, freed from constraints exerted by surrounding material, remains flat at equilibrium), the energies per surface unit that are to be considered in this surface model are of two kinds: firstly, a curvature term that can express $\frac{1}{2}\kappa c^2 + \overline{\kappa} g$ [10, 26], where $c = \frac{1}{R_1} + \frac{1}{R_2}$ and $g = \frac{1}{R_1} \times \frac{1}{R_2}$ are, respectively, the mean and Gaussian curvatures (R_1 and R_2 being the local principal curvature radii), and κ and $\overline{\kappa}$ are, respectively, the mean and Gaussian curvature constants[2]. The other term may be written, in a Hookean linear model: $\frac{1}{2}\epsilon_{ij} K_{ijkl} \epsilon_{kl}$, where ϵ_{ij} and K_{ijkl}, respectively, represent the two-dimensional strain and elasticity tensors for in-plane deformations. For a homogeneous and isotropic surface, the non-zero terms of the two-dimensional elasticity tensor are $K_{xxxx} = K_{yyyy} = \frac{Y_{2\mathrm{D}}}{1-\nu_{2\mathrm{D}}^2}$, $K_{xxyy} = K_{yyxx} = \frac{\nu_{2\mathrm{D}}\, Y_{2\mathrm{D}}}{1-\nu_{2\mathrm{D}}^2}$ and $K_{xyxy} = K_{yxyx} = \frac{Y_{2\mathrm{D}}}{1+\nu_{2\mathrm{D}}}$, with $Y_{2\mathrm{D}}$ the two-dimensional Young modulus and $\nu_{2\mathrm{D}}$ the two-dimensional Poisson ratio, which is comprised between -1 and 1 [10]. This in-plane elasticity term can be rewritten as $\frac{Y_{2\mathrm{D}}}{2(1+\nu_{2\mathrm{D}})}\left[\mathrm{Tr}(\epsilon^2) + \frac{\nu_{2\mathrm{D}}(\mathrm{Tr}\,\epsilon)^2}{1-\nu_{2\mathrm{D}}}\right]$ for the sake of concision.

In a linear approximation, the relation between the 2D parameters and the 3D features of the plate (Young modulus $Y_{3\mathrm{D}}$, Poisson's ratio $\nu_{3\mathrm{D}}$, thickness d) with zero boundary tangential constraints [10] is expressed as (detailed, *e.g.*, in [23] or [7]):

$$\nu_{2\mathrm{D}} = \nu_{3\mathrm{D}} = \nu, \tag{1}$$

$$Y_{2\mathrm{D}} = Y_{3\mathrm{D}} d, \tag{2}$$

$$\kappa = \frac{Y_{3\mathrm{D}}}{12\,(1-\nu^2)}\, d^3, \tag{3}$$

$$\overline{\kappa} = (\nu - 1)\,\kappa = -\frac{Y_{3\mathrm{D}}}{12\,(1+\nu)}\, d^3. \tag{4}$$

Since for bulk materials the maximum value of $\nu_{3\mathrm{D}}$ is $\frac{1}{2}$ for thermodynamic reasons [10], one can notice that the range of 2D Poisson's ratio that effectively describes a thin plate of an isotropic material is limited to a maximum value of $\frac{1}{2}$. In other terms, even a thin plate of an incompressible isotropic material cannot behave as an incompressible surface (where $\nu_{2\mathrm{D}} = 1$), thanks to the possibility of having its thickness varied. On the other limit,

[2] There may be discrepancies between different communities about the definitions of both κ and c. Here we used definitions that rule in the Soft Matter community, and more particularly in physics of lipids vesicles: $c = \frac{1}{R_1} + \frac{1}{R_2}$, where R_1 and R_2 are the main algebraic curvature radii (mathematicians usually consider half of this quantity). And we take κ such that the bending energy of a sphere is $8\pi\kappa$.

Poisson's ratio can reach -1 as a lower value, but negative values correspond to less common "auxetic" materials.

Conversely the thickness of the plate, as a function of 2D parameters, writes

$$d = \sqrt{12\left(1-\nu^2\right)\frac{\kappa}{Y_{2\mathrm{D}}}}\,. \tag{5}$$

For describing surfaces with asymmetric properties, the notion of "spontaneous curvature" was introduced by W. Helfrich [26]. It was recently shown that to describe the deformations of an initially stress-free thin shell of radius R, the three contributions (in-plane, mean curvature and Gaussian energy, that may have a non-vanishing part even for closed surfaces, depending on the definition of a non-zero spontaneous curvature) can be rewritten in an easily computable way as [27]

$$E_{\mathrm{elastic}} = \mathrm{const} + \int_{\mathrm{shell\ surface}} \left[\frac{1}{2}\kappa\left(c-c_0^*\right)^2 + \frac{1}{2}\epsilon_{ij}K_{ijkl}\epsilon_{kl} + \gamma_{\mathrm{eff}}\right]\mathrm{d}S, \tag{6}$$

with $c_0^* = \frac{1+\nu}{R}$ being the effective spontaneous curvature, and $\gamma_{\mathrm{eff}} = -\frac{(1+\nu)\kappa}{2R^2}$ an effective surface tension.

This expression is slightly different from the one used in [20], hence we will quantitatively discuss, in the results, modifications induced by the use of this more complete expression.

More generally, we will consider the influence of sphere size through the use of the adimensionalized Föppl-von Kármán number [28] $\gamma = \frac{Y_{2\mathrm{D}}R^2}{\kappa}$, that gives the order of magnitude of the ratio between in-plane and out-of plane deformation energies [23]. An elastic surface with the energy given in eq. (6) can effectively describe a thin shell of an isotropic material if $12(1-\nu^2)/\gamma \ll 1$, in addition to the condition $\nu_{2\mathrm{D}} \leq \frac{1}{2}$. In this range, γ roughly scales like $(\frac{R}{d})^2$. Out of this range, such a surface model does not correspond to any thin shell of an isotropic material; it can nevertheless describe different types of objects, *e.g.* gel-phase vesicles [17] that can hence be considered as thin shells of non-isotropic materials.

Numerical experiments are performed by minimizing the elastic energy as expressed in eq. (6) for different inner volumes, with the free software Surface Evolver [29]. A whole in-silico deflation experiment (from $V_{\mathrm{init}} = \frac{4}{3}\pi R^3$ to $\approx 0.2 \times V_{\mathrm{init}}$) is realized through a succession of different equilibrium states, these latter found according the process described in [20], and calculated successively for inner volumes decreased by steps of at maximum 2% of the initial volume (steps amplitude is reduced in some situations in order to avoid the nucleation of secondary dimples).

3 First-order transition toward axisymmetric depression

Deflation of a spherical elastic surface, at imposed either volume or external pressure, causes an abrupt buckling from the spherical conformation in order to release in-plane compressive stress. The purpose here is to compare the numerical approach described in the previous paragraph to known features of this buckling, for the range of parameters that scans the generality of thin shells of isotropic material.

3.1 Buckling pressure

First, buckling relaxes in-plane constraints, and causes a drastic drop of the inside/outside pressure difference $\Delta P = P_{\mathrm{ext}} - P_{\mathrm{int}}$. Figure 1 displays typical evolutions for the pressure difference: first a linear increase followed by a drop at first buckling, after which pressure difference varies in a much lesser extent. Linear behaviour is expected before the first buckling due to the relation between pressure and elastic energy $P_{\mathrm{ext}} - P_{\mathrm{int}} = \partial E_{\mathrm{elastic}}/\partial(\Delta V)$ (detailed in [7]), and quadratic dependence of E_{elastic} with $\Delta V = V_{\mathrm{init}} - V$ (see, *e.g.*, [20]).

In the simulations presented here, designed not to be stuck in multi-indentation conformations of higher energy, or other less stable, the first buckling leads to a single axisymmetric dimple. It is expected to happen when the external overpressure $\Delta P = P_{\mathrm{ext}} - P_{\mathrm{int}}$ reaches the critical value [11,12]

$$\Delta P_c = 2\left[3\left(1-\nu^2\right)\right]^{-1/2} \times Y_{3\mathrm{D}}\left(\frac{d}{R}\right)^2. \tag{7}$$

As expected, the first buckling in our simulations effectively occurs at a pressure difference of order $\Delta P_{\mathrm{Landau}} = Y_{3\mathrm{D}}(\frac{d}{R})^2$ (sect. 1). For a given Poisson's ratio, the uncertainty due to discrete volume increments does not allow to conclude that $\Delta P_{\mathrm{buckling1}}/\Delta P_{\mathrm{Landau}}$ is affected by γ (see, *e.g.*, fig. 1 displaying several cases at $\nu = -0.5$). The effect of Poisson's ratio is displayed in fig. 2: it shows that the pressure which induces buckling in our simulations quantitatively follows the theoretical equation (7), which reinforces the validity of our approach.

3.2 Buckling volume

The mechanism of buckling in axisymmetric conformations was quite recently investigated in detail by Knoche *et al.* [12], with the study of various metastability branches. At first significative order, their calculations show that for the trivial isotropic ("spherical") deformation, the relative volume variation due to an external overpressure $\Delta P = P_{\mathrm{ext}} - P_{\mathrm{int}}$ is expressed as

$$\frac{\Delta V}{V} = \frac{3\left(1-\nu\right)}{2} \times \frac{R}{d} \times \frac{\Delta P}{Y_{3\mathrm{D}}}\,.$$

Hence the deflation at buckling pressure writes [11,12]

$$\left(\frac{\Delta V}{V}\right)_{\mathrm{buck\,1}} = \sqrt{3\left(\frac{1-\nu}{1+\nu}\right)} \times \frac{d}{R}\,. \tag{8}$$

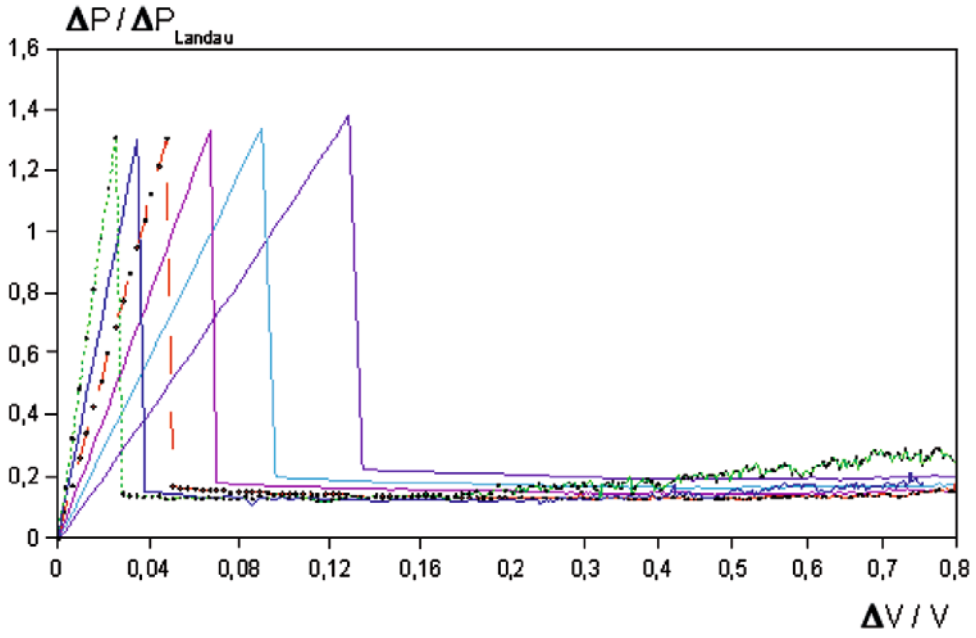

Fig. 1. (Colour on-line) Pressure difference $\Delta P = P_{\rm ext} - P_{\rm int}$ adimensionalized by $\Delta P_{\rm Landau} = Y_{\rm 3D}(\frac{d}{R})^2$ (or $[12\,Y_{\rm 2D}\kappa(1-\nu^2)]^{1/2}/R^2$ in 2D parameters), as a function of the relative volume variation, for surfaces of similar Poisson's ratio $\nu = -0.5$. Dotted green: $\gamma = 1.17\times10^5$ ($\frac{d}{R} = 8.8\times10^{-3}$); blue: $\gamma = 6.07\times10^4$ ($\frac{d}{R} = 1.22\times10^{-2}$), long-dashed orange: $\gamma = 3.22\times10^4$ ($\frac{d}{R} = 1.67\times10^{-2}$), magenta: $\gamma = 1.17\times10^4$ ($\frac{d}{R} = 2.31\times10^{-2}$), light blue: $\gamma = 9.33\times10^3$ ($\frac{d}{R} = 3.11\times10^{-2}$), violet: $\gamma = 4.67\times10^3$ ($\frac{d}{R} = 4.39\times10^{-2}$). Notice the scale switch at $\frac{\Delta V}{V} = 0.2$. Points (corresponding each to a minimization) emphasize two curves with typical behaviour after buckling: increasing (green curve), and plateauing (orange).

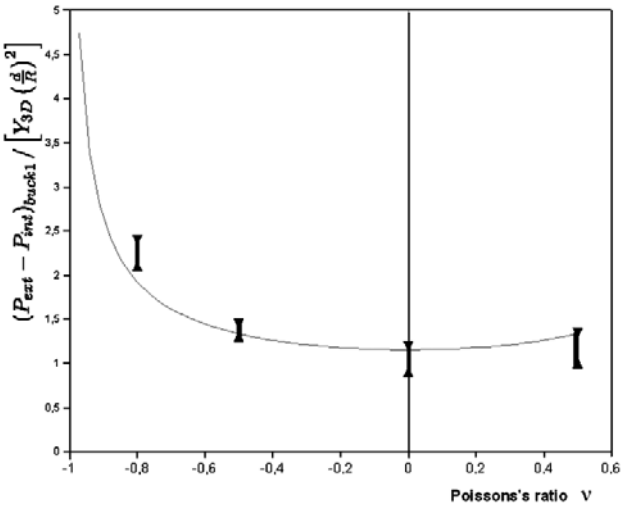

Fig. 2. Pressure $(\Delta P)_{\rm buck\,1} = (P_{\rm ext}{-}P_{\rm int})_{\rm buck\,1}$ at first sphere$\rightarrow$bowl buckling, adimensionized by $\Delta P_{\rm Landau}$. Error bars represent the range of this quantity for γ between 4.67×10^3 and 2.33×10^5. Line: theoretical value $2[3(1-\nu^2)]^{-1/2}$, from eq. (7).

Figure 3 presents values of $(\frac{\Delta V}{V})_{\rm buck\,1}$ from numerical simulations, as a function of a combination of γ and ν translated in 3D parameters: here also the theoretical equation (8) is quantitatively retrieved. One may notice (since by essence $(\frac{\Delta V}{V})_{\rm buck\,1} \leq 1$) that the sphere $\rightarrow$ bowl transition vanishes for $\frac{d}{R} \geq \sqrt{(1+\nu)/3(1-\nu)}$, which indicates a destabilization of the axisymmetric bowl for the most auxetic materials. This was qualitatively expected from the κ divergence in this limit, which makes curvature deformations prohibitive compared to in-plane compressions[3].

Using the 2D parameters of the surface model, relation (8) also writes:

$$\left(\frac{\Delta V}{V}\right)_{\rm buck\,1} = 6\,(1-\nu)\,\gamma^{-\frac{1}{2}}\,. \qquad (9)$$

Extending our purpose out of the range of 2D parameters that effectively can describe a thin shell of isotropic material, we may remark that extrapolation to $\nu = 1$ induces vanishing of $(\frac{\Delta V}{V})_{\rm buck\,1}$, and hence destabilization of the spherical conformation: this limit corresponds to incompressible surfaces, that will necessarily undergo a deformation implying curvature even for the smallest volume decreases, since area variation is prohibited. For the thickest shells, *i.e.* $\gamma \lesssim 80$, shape transition occurs not any more through sudden inversion of a spherical cap, but by slowly deforming into an ovoid, that flattens at the location of future depression under further deflation. We did not, here, specifically study this extreme behaviour.

For practical purposes, we may notice that the large range of parameters explored shows that in terms of volume, the onset of buckling mainly depends on the relative

[3] A possible expression of the 2D compressibility modulus is $\chi_{\rm 2D} = \frac{Y_{\rm 2D}}{2(1-\nu)} = \frac{Y_{\rm 3D}\times d}{2(1-\nu)}$.

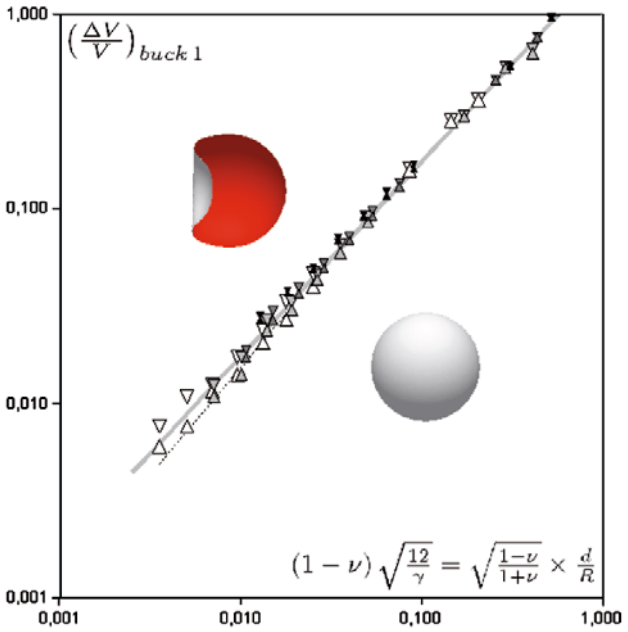

Fig. 3. Relative volume variation $(\frac{\Delta V}{V})_{\mathrm{buck\,1}}$ at the sphere → bowl buckling (lower and upper limit of the error bars are indicated, respectively, by upward and downmard triangles). White: $\nu = 0.5$; light gray: $\nu = 0$; dark grey: $\nu = -0.5$; black: $\nu = -0.8$. Grey line: $(\frac{\Delta V}{V})_{\mathrm{buck\,1}} = 6(1-\nu)\gamma^{-\frac{1}{2}}$ (this is eq. (8) expressed in 2D parameters). Dotted line: relation established in [20] for $\nu = 1/3$: taking into account the Gaussian curvature, the elastic energy increases the volume threshold by at maximum 20% for the thinnest shells of the shells previously studied. Illustrative inserts display deflated spherical surfaces at $\gamma = 4666$ and $\nu = -0.8$ (hence $\frac{d}{R} = 0.0304$), with relative volume variations, respectively, $\frac{\Delta V}{V} = 0.161$ (spherical) and 0.167 (buckled, section view, same scale).

thickness $\frac{d}{R}$, with only a weak influence of Poisson's ratio. Since this latter ranges between 0 and $\frac{1}{2}$ for common materials (*i.e.* non auxetic, with $\nu \geq 0$), the prefactor of $\frac{d}{R}$ varies between $\sqrt{3}$ and 1, which is much narrower than the range in $\frac{d}{R}$ that can be explored.

4 Second-order transition toward polygonal depression

4.1 Location of the transition

In the axisymmetric bowl shape, global bending of the rim on the equator costs in-plane deformation: extension on the outer side of the rim, and compression on the inner one. For the thinnest shells, compressive stress parallel to the equator leads to a secondary buckling, where the inner side of the rim undulates to adapt to axial compression (fig. 4, left), forming folds, or "wrinkles", that deform the axisymmetric depression into a roughly polygonal shape (fig. 4, right). Such a conformation mainly involves curvature deformations, much less energetic [23] than compression energy that quadratically increases with $\frac{\Delta V}{V}$. Figure 5

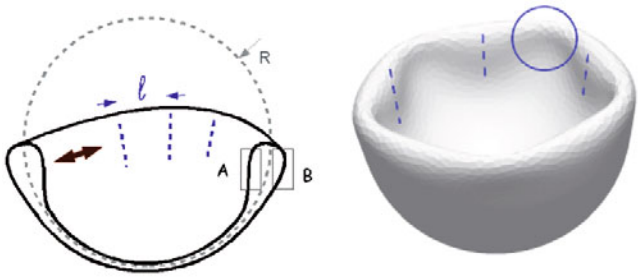

Fig. 4. (Colour on-line) Left: schematisation of a spherical surface near complete deflation. The inner part of the rim endures a compressive stress in the direction indicated by the red double arrow. Relaxation of in-plane deformation occurs, for the thinnest shells, via undulation deformation, generating wrinkles (folds) all along the rim (examples schematized with blue dashed lines). Length ℓ stands for lateral extension of the wrinkles. Right: simulation with $\gamma = 9.33\times10^3$, $\nu = 0.5$ ($\frac{d}{R} = 0.031$) and $\frac{\Delta V}{V} = 0.562$. Maxima of undulation are stressed with blue dashed lines; the circle locates the zone of high curvature that forms the apex of the *s*-cone.

shows how elastic energy dispatches between in-plane and out-of-plane deformation energies in a typical numerical deflation. Wrinkles match with the rim through a zone of high curvature that has a folding role similar to what realizes the apex of *d*-cones [30–32], except that the surface is not developable but is spherical, hence the concept of "*s*-cones" proposed by Reis and Lazarus [33].

Secondary buckling from axisymmetric bowl shape to polygonal indentation, quite smooth, is harder to detect than the first one (fig. 5). The corresponding relative volume variation $(\frac{\Delta V}{V})_{\mathrm{buck\,2}}$ is determined on the one hand by the maximum deflation before loss of axisymmetry, and on the other hand by the $\frac{\Delta V}{V}$ at which the rim presents convex zones under axial observation (as shown on the lower part of fig. 5, subfigure c). Figure 6 presents a typical shape phase diagram for $\nu = -0.5$, with three distinct zones: spherical coformation, axisymmetric bowl and wrinkled depression. One may notice that for the thinnest shells, the incremented deflation we numerically performed shows a direct transition from the sphere to the wrinkled bowl. Relative volume variation at first buckling nevertheless obeys a single power law on the whole range of relative thicknesses. We focus in this section on the second buckling, hence considering only deflations where wrinkles appear on an already existing axisymmetric conformation. Figure 7 displays how $(\frac{\Delta V}{V})_{\mathrm{buck\,2}}$ varies with the Föppl-von Karmán number γ for different Poisson's ratios. Data indicate a dependence on γ, but scattering prevents from concluding on an influence by ν; linear regression on logarithms[4] provides a correlation coefficient of −0.99:

$$\left(\frac{\Delta V}{V}\right)_{\mathrm{buck\,2}} = 8470 \times \gamma^{-1.085}. \qquad (10)$$

[4] Plotting $\ln\{(\frac{\Delta V}{V})_{\mathrm{buck\,2}}\}$ *versus* $\ln(\frac{d}{R})$, as for the first buckling, excessively particularizes points at $\nu = -0.8$, which results in a correlation coefficient of only −0.90.

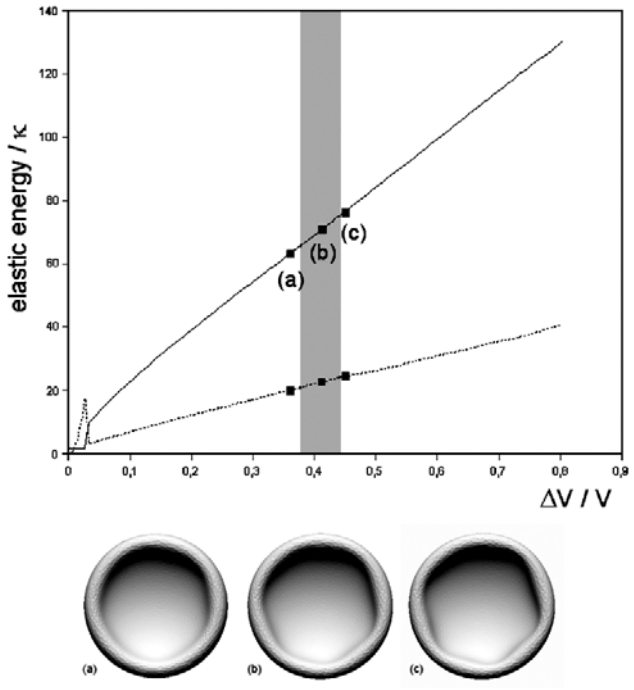

Fig. 5. Deformation energies at different relative volume variations (volume step $\approx 0.6\%$ of the initial volume), adimensionalized by the curvature constant κ, for $\gamma = 9.33 \times 10^3$ and $\nu = 0.5$ ($\frac{d}{R} = 0.031$). Dashed line: Hookean in-plane deformation energy, linked to the second significative term of eq. (6), *i.e.* $\frac{1}{2}\epsilon_{ij}K_{ijkl}\epsilon_{kl}$. Grey continuous line: elastic energy linked to the first significative term: $\frac{1}{2}\kappa(c - c_0^*)^2$. This term does not vanish at $\frac{\Delta V}{V} = 0$ because $c_0^* \neq 1/R$; in the total elastic energy, it is counterbalanced by the const and the effective surface term expressed by γ_{eff} in eq. (6). Effective surface energy (not represented here) varies at maximum by $-0.33\,\kappa$, and on an amplitude $0.03\,\kappa$ in the non-spherical conformations. Grey zone indicates the second transition from axisymmetric bowl shape to depression with inner wrinkles ("polygonal indentation" [18]), determined as explained in the text. First transition from sphere to axisymmetric bowl occurs through abrupt decrease of the in-plane deformation energy, at $\frac{\Delta V}{V} = 0.03$.

This expression is compatible with previous results obtained for $\nu = 1/3$ with slightly different numerical models: the shell without Gaussian curvature evoked in sect. 2, [20], and the spring model without spontaneous mean curvature of ref. [18] (both are represented in fig. 7 for their range of validity).

Extrapolating eq. (10) up to $\frac{\Delta V}{V} = 1$ suggests that this secondary buckling does not happen, *i.e.* single indentation keeps its axisymmetry, below a threshold value $\gamma_{c,\text{buck 2}} = 4170$. In tridimensional parameters, relation (10) expresses as

$$\left(\frac{\Delta V}{V}\right)_{\text{buck 2}} = 571 \times \left(\frac{d/R}{\sqrt{1-\nu^2}}\right)^{2.17}. \qquad (11)$$

The dependence in ν for non-auxetic materials is even weaker than for the axisymmetric buckling since it plays at maximum by a factor 4/3. Besides, for the range of Poisson's ratio studied here, there is no axisymmetric conformation to be expected for $d/R < 0.003$. Relation (11) also implies that wrinkles are not expected when $d/R \gtrsim 0.054 \times \sqrt{1-\nu^2}$: a particular consequence is that in wrinkles prevention, a very auxetic material (with $\nu \to -1$) may help.

4.2 Characterization of buckled shapes with the number of wrinkles

For the thinnest shells that undergo polygonal indentation, the most conspicuous feature is the number W of wrinkles, or s-cones. Figure 8 shows the evolution of W for a typical deflation: first does W decrease while the freshly nucleated and still very flat depression hollows and enlarges, then it increases again. Data are quite scattered: there is a typical noise of order ± 1 on W, that has no observable correspondence in smooth energy curves (fig. 5). In order to decrease data scattering, we calculated W_{deflated} as the average value of W between $\frac{\Delta V}{V} = 0.53$ and $\frac{\Delta V}{V} = 0.76$ (these values have been choosen in order to cover, for all the simulations, a significant range of relative volume variation before autocontact, this latter happening around $\frac{\Delta V}{V} \approx 0.9$). Values of W_{deflated} are comparable with results from the previous model, which did not take Gaussian curvature into account, and indicated a scaling law in $\gamma^{-1/4}$ [7,20]. The dependence of W_{deflated} with γ and ν is shown in fig. 9, expressed in 3D parameters. It shows a scaling in $(\frac{d}{R})^{-1/2}$, which provides clues on the typical transversal size l of the s-cones (presented in fig. 4, left). Since s-cones stand alongside one another on a length which is of the order of an equator, we can estimate l as $\frac{2\pi R}{W_{\text{deflated}}}$. Hence the best fit of W_{deflated} as linear with $(\frac{d}{R})^{-1/2}$ (fig. 9) can be expressed as

$$l \approx 6.7\sqrt{dR}. \qquad (12)$$

This result is fully comparable to the wrinkles wavelength $4.7\sqrt{dR}$ that can be calculated from recent results by Vella *et al.* [34] on the indentation of strongly pressurized shells. As shown in ref. [10], $\sqrt{dR}$ arises naturally from balancing the bending and in-plane deformation energy of a small deformation on a spherical shell. Recent results by [12] showed that $\sqrt{dR}$ scales also for the rim width even in large axisymmetric depressions; we confirm here that it governs also other types of large deformations such as s-cones transversal size in polygonal depressions.

5 Other postbuckling features

First buckling and its consequences were presented in sect. 3. For application purpose, we may focus on the inside/outside pressure difference after its drop at first buckling. Careful examination of the numerical data revealed supplementary features, uncorrelated with the occurrence

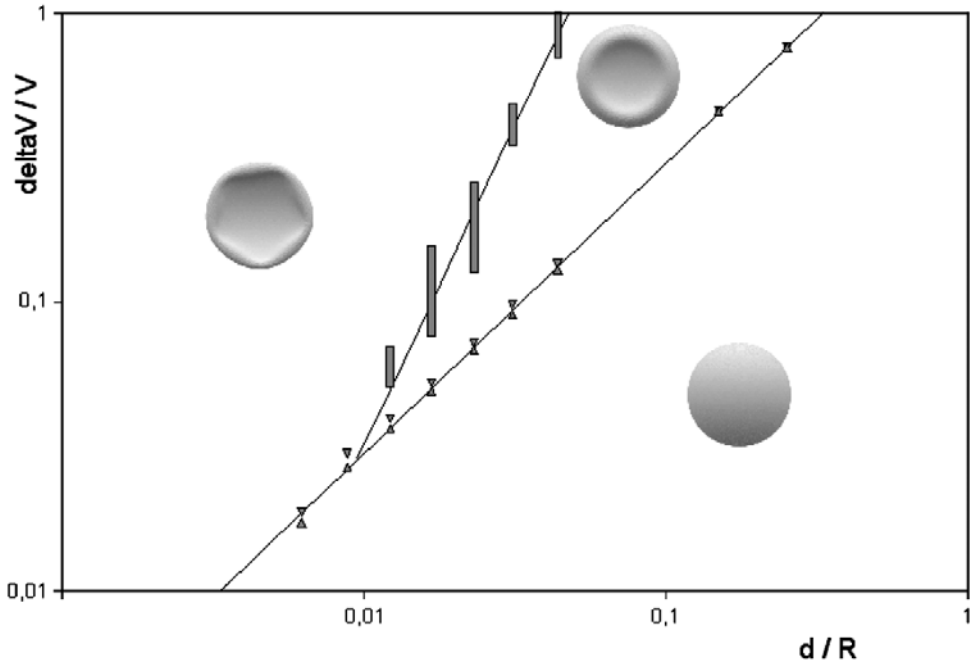

Fig. 6. Shapes in the relative thickness/relative volume variation phase diagram, for: $\nu = -0.5$. Illustrations: shells with $d/R = 0.031$ and $\nu = -0.5$ ($\frac{\Delta V}{V} = 0$, 0.20 and 0.55).

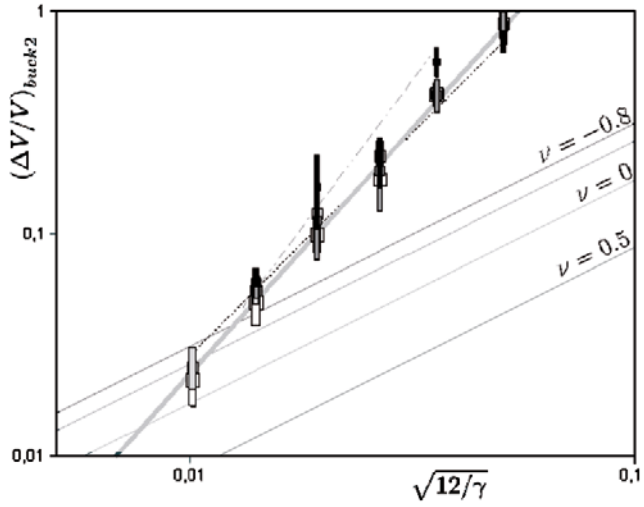

Fig. 7. Points: relative volume variation at which the axisymmetric depression becomes "polygonal", *versus* $\sqrt{12/\gamma}$ (which is to be identified with d/R when $\nu = 0$). White: $\nu = 0.5$; light grey: $\nu = 0$; dark grey: $\nu = -0.5$; black: $\nu = -0.8$. Thick grey line: eq. (11). Continuous lines indicate the location of the first-order buckling for different Poisson's ratio (from eq. (8)), under which only the spherical conformation is to be found. Non-continuous lines: in their domain of validity, equations describing the axisymmetric/wrinkled bowl transition published in previous works for $\nu = 1/3$ (see text): dotted black refers to [20], dashed grey to [18].

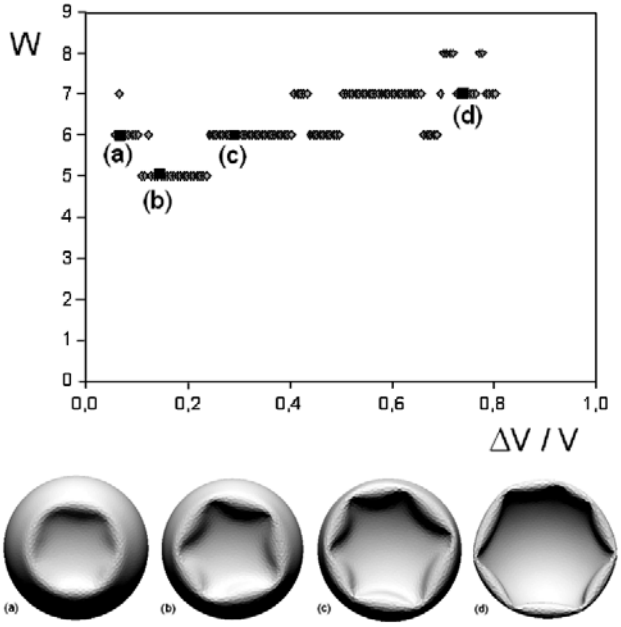

Fig. 8. Number of wrinkles (s-cones) held by the single depression after the secondary buckling of fig. 5. Poisson's ratio $\nu = 0.5$; Föppl-von Karman number $\gamma = 6.06 \times 10^4$ ($\frac{d}{R} = 0.0122$). Lower part: conformations at points indicated in the main figure.

of the secondary buckling previously exposed: two types of behaviour clearly appear in the evolution of the reduced pressure $\frac{\Delta P}{\Delta P_{\text{Landau}}}$ during deflation.

For $\frac{d}{R} \gtrsim 0.014$, the pressure difference ΔP presents the type of evolution calculated by [12], *i.e.* quasi-plateauing after buckling (variation of about 15% during the whole

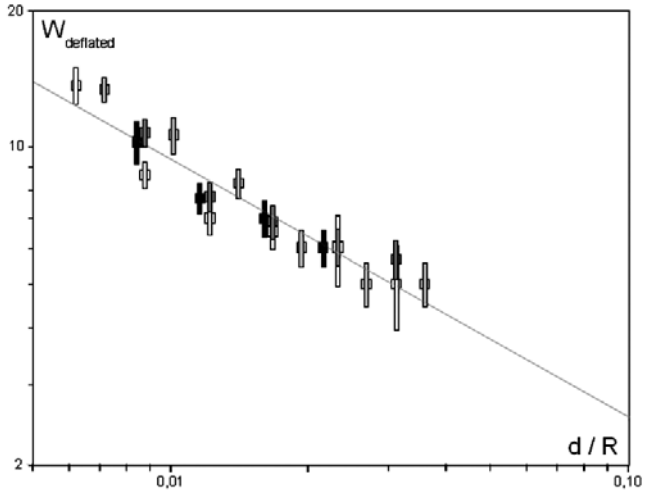

Fig. 9. Number W_{deflated} of wrinkles (s-cones) at the end of a numerical deflation (averaged between $\frac{\Delta V}{V} = 0.53$ and $\frac{\Delta V}{V} = 0.76$). Error bars are taken as the standard deviation on this range, with a minimum value of ± 0.5. White: $\nu = 0.5$; light grey: $\nu = 0$; dark grey: $\nu = -0.5$; black: $\nu = -0.8$. Continuous line: $W_{\mathrm{deflated}} = 0.940 \times (\frac{d}{R})^{-\frac{1}{2}}$.

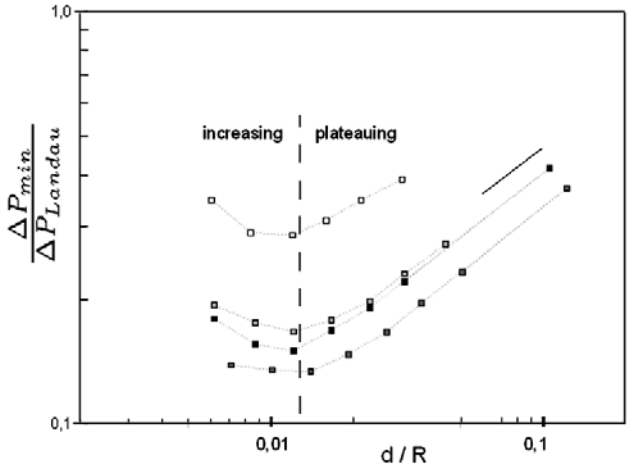

Fig. 10. Minimum inside/outside pressure difference after buckling (cf. fig. 1), adimensionalized by Landau pressure, logarithmic representation. Black: $\nu = 0.5$; dark grey: $\nu = 0$; light grey: $\nu = -0.5$; white: $\nu = -0.8$. Dashed line separates the two types of evolution of the pressure after the first buckling: increasing or plateauing (see fig. 1). Black line indicates slope 0.5.

deflation, plus some occasional dispersion due to numerical procedure), up to autocontact. Furthermore, an order relation is respected: at every volume step, the ratio $\frac{\Delta P}{\Delta P_{\mathrm{Landau}}}$ weakly increases when γ decreases. This is to be observed in fig. 1, for the 4 curves corresponding to the highest relative thicknesses.

For the thinnest shells ($\frac{d}{R} \lesssim 0.012$ in the simulations performed), $\frac{\Delta P}{\Delta P_{\mathrm{Landau}}}$ regularly re-increases with deflation after the pressure drop, crossing successively the curves at smaller γ's (as shown on the 2 "thinnest" curves of fig. 1).

In order to extract a general behaviour from these differents observations, we focused on $\frac{\Delta P_{\mathrm{min}}}{\Delta P_{\mathrm{Landau}}}$, the minimum value of $\frac{\Delta P}{\Delta P_{\mathrm{Landau}}}$ after buckling. Figure 10 shows that the cross-over between the two regimes around $\frac{d}{R} \approx 0.014$ also corresponds, for each ν, to the minimum of relative pressure drop after the first buckling. In the plateauing regime, $\frac{\Delta P_{\mathrm{min}}}{\Delta P_{\mathrm{Landau}}}$ stands for the plateauing value for $\frac{d}{R} \gtrsim 0.014$; it shows a power law of the type $\frac{\Delta P_{\mathrm{min}}}{\Delta P_{\mathrm{Landau}}} = a(\nu) \times (\frac{d}{R})^{0.5}$. Similarly to what was done in sect. 3, and since $a(\nu)$ appears to be even (curves at $\nu = 0.5$ and $\nu = -0.5$ almost mix up in fig. 10), we looked for a prefactor of the form $(1-\nu^2)^x$, minimizing x for the best fits at $\frac{d}{R} > 0.014$. This led us to propose the master curve presented in fig. 11, of formula $\frac{\Delta P_{\mathrm{min}}}{Y_{\mathrm{3D}}} \times (1-\nu^2)^{0.773} = 0.75 \times (\frac{d}{R})^{2.5}$. We do not have for the moment theoretical clues to justify these two successive fitting operations, but i) it allows to describe numerical results in a very condensed way for $\frac{d}{R} \geq 0.014$, and ii) for all the shells these reduced values impressively gather on a single curve, for γ ranging from 8×10^2 to 4.7×10^5, and for ν between -0.8 and 0.5. This result, exposed in fig. 11 using 3D parameters, is expected to be of practical use for all experiments involving deflation con-

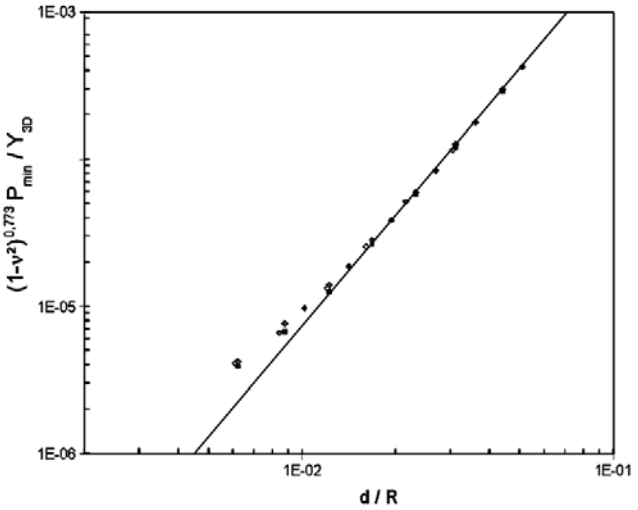

Fig. 11. Pressure master curve after first buckling: $\frac{\Delta P_{\mathrm{min}}}{Y_{\mathrm{3D}}} \times (1-\nu^2)^{0.773}$ *versus* $\frac{d}{R}$. Black squares: $\nu = 0.5$; black diamonds: $\nu = 0$; light grey diamonds: $\nu = -0.5$; white diamonds: $\nu = -0.8$. Continuous line: $\frac{\Delta P_{\mathrm{min}}}{Y_{\mathrm{3D}}} \times (1-\nu^2)^{0.773} = 0.75 \times (\frac{d}{R})^{2.5}$.

trolled by the volume. On a more conceptual point of view, plot clearly confirms two different scalings of the pressure during deflation, around a threshold in relative thickness $(\frac{d}{R})_c \approx 0.013$. This may be an indication of the existence of different ways to accommodate s-cones on a sphere, and requires further investigations.

6 Conclusion

Systematic numerical study of the buckling of a spherical shell, in the conformation with a single depression,

allows to sketch the influence of the different geometrical or elastic parameters through quite simple theoretical or phenomenological laws. The surface model can be translated in 3D parameters, that are the shell's thickness, and the two elastic parameters of the material that compose it: Young modulus and Poisson's ratio.

At imposed volume, the Young modulus does not play on the shape. Results showed that the first transition (toward axysimmetrically buckled shape), and the second one, with appearance of wrinkles, or "*s*-cones", is mainly driven by $\frac{d}{R}$ for non-auxetic (*i.e.* with positive Poisson's ratio) materials. For auxetic materials, Poisson's ratio may have a determining importance, by strongly displacing transitions toward higher values of the relative volume variation, up to possible vanishing. Decreasing Poisson's ratio down to very negative values stabilizes spherical deflation at the expense of dimples creation, and axisymmetric dimples against appearance of wrinkles.

The number of wrinkles indicates a dependence on $(\frac{d}{R})^{-1/2}$, that confirms $\sqrt{dR}$ as the accurate scaling for elastic deformations of elastic spherical surfaces.

The Young modulus scales pressure features: critical inside/outside pressure difference that triggers first buckling, and plateauing pressure after buckling. Detailed behaviour, that is shown to reduce to a master curve, opens the possibility for two different wrinkling regimes.

The author thanks K. Brakke for developing and maintaining the Surface Evolver software, including invaluable interactions during this work, and P. Marmottant and F. Quéméneur for fruitful discussions.

References

1. S. Sacanna, W.T.M. Irvine, L. Rossi, D.J. Pine, Soft Matter **7**, 1631 (2011).
2. Z. Sun, Y. Luo, Soft Matter **7**, 871 (2011).
3. N. Tsapis, E.R. Dufresne, S.S. Sinha, C.S. Riera, J.W. Hutchinson, L. Mahadevan, D.A. Weitz, Phys. Rev. Lett. **94**, 018302 (2005).
4. J. Bahadur, D. Sen, S. Mazumder, B. Paul, H. Batt, S.G. Singh, Langmuir **28**, 1914 (2012).
5. M. Delcea, H. Möhwald, A.G. Skirtach, Adv. Drug Delivery Rev. **63**, 730 (2011).
6. M.V. Kiryukhin, S.M. Man, S.R. Gorelik, G.S. Subramanian, H.Y. Low, G.B. Sukhorulov, Soft Matter **7**, 6550 (2011).
7. P. Marmottant, A. Bouakaz, N. De Jong, C. Quilliet, J. Acoust. Soc. Am. **129**, 1231 (2011).
8. E. Katifori, S. Alben, E. Cerda, D.R. Nelson, J. Dumais, Proc. Natl. Acad. Sci. U.S.A. **107**, 7635 (2010).
9. A.V. Pogorelov, *Bending of Surfaces and Stability of Shells* (American Mathematical Society, Providence, 1988).
10. L. Landau, E.M. Lifschitz, *Theory of Elasticity*, 3rd edition (Elsevier Butterworth-Heinemann, Oxford, 1986).
11. J.W. Hutchinson, J. Appl. Mech. **34**, 49 (1967).
12. S. Knoche, J. Kierfeld, Phys. Rev. E **84**, 046608 (2011).
13. R.L. Carlson, R.L. Sendelbeck, N.J. Hoff, Exp. Mech. **7**, 281 (1967).
14. C.I. Zoldesi, A.I. Imhof, Adv. Mater. **17**, 924 (2005).
15. S.S. Datta, H.C. Shum, D.A. Weitz, Langmuir **26**, 18612 (2010).
16. D. Sen, J.S. Melo, J. Bahadur, S. Mazumder, S. Bhattacharya, G. Gosh, D. Dutta, S.F. D'Souza, Eur. Phys. J. B **31**, 393 (2010).
17. F. Quéméneur, C. Quilliet, M. Faivre, A. Viallat, B. Pépin-Donat, Phys. Rev. Lett. **108**, 108303 (2012).
18. G.A. Vliegenthart, G. Gompper, New J. Phys. **13**, 045020 (2011).
19. M. Okubo, H. Minami, K. Morikawa, Colloid Polym. Sci. **279**, 931 (2001).
20. C. Quilliet, C. Zoldesi, C. Riera, A. van Blaaderen, A. Imhof, Eur. Phys. J. E **27**, 13 (2008) and **32**, 419 (2010).
21. L. Pauchard, S. Rica, Philos. Mag. B **78**, 225 (1998).
22. A. Vaziri, Thin-Walled Struct. **47**, 692 (2009).
23. S. Komura, K. Tamura, T. Kato, Eur. J. Phys. E **18**, 343 (2005).
24. C. Quilliet, Phys. Rev. E **74**, 046608 (2006).
25. B. Audoly, Y. Pomeau, *Elasticity and Geometry: From Hair Curls to the Nonlinear Response of Shells* (Oxford University Press, 2010).
26. W. Helfrich, Z. Naturforsch. C **28**, 693 (1973).
27. P. Marmottant, A. Farutin, C. Misbah, C. Quilliet, submitted.
28. J. Lidmar, L. Mirny, D.R. Nelson, Phys. Rev. E **68**, 051910 (2003).
29. K. Brakke, Exp. Math. **1**, 141 (1992).
30. L. Pauchard, Y. Pomeau, S. Rica, C. R. Acad. Sci. (Paris) IIb **323**, 411 (1997).
31. S. Chaïeb, F. Melo, J.-C. Géminard, Phys. Rev. Lett. **80**, 2354 (1998).
32. E. Cerda, L. Mahadevan, Proc. R. Soc. London, Ser. A **461**, 671 (2005).
33. A. Lazarus, P. Reis, private communication.
34. D. Vella, A. Ajdari, A. Vaziri, A. Boudaoud, Phys. Rev. Lett. **107**, 174301 (2011).